ARTICLE

OPEN

Check for updates

Mechanics of coseismic and postseismic acceleration of active landslides

Marc Kohler [1✉] & Alexander M. Puzrin [1]

Active slow-moving landslides exhibit very different coseismic and postseismic behaviour. Whereas some landslides do not show any postseismic acceleration, there are many that experience an increased motion in the days to weeks following an earthquake. The reason for this behaviour remains debated and the underlying mechanisms are only partially understood. In recent years, it has been suggested that postseismic acceleration is caused by excess pore water pressures generated outside of the shear zone during seismic shaking, with their subsequent diffusion into the shear zone. Here we show that this hypothesis is indeed plausible and hydro-mechanically consistent by using a basic rate-dependent physical landslide model. Our simulations provide insight into the landslide behaviour in response to seismic shaking and its main controlling parameters: preseismic landslide velocity, rate-dependency of soil strength in the shear zone, hydro-mechanical characteristics of the adjacent soil layers and the earthquake intensity.

[1] Institute of Geotechnical Engineering, ETH Zurich, Switzerland. ✉email: marc.kohler@igt.baug.ethz.ch

Landslides are one of the major threats in mountainous regions causing thousands of fatalities every year[1]. Besides precipitation, landslide activity can be strongly influenced by earthquakes[2,3]. Of particular interest is the response to seismic shaking of active slow-moving landslides, which pose a serious threat to people and infrastructure[4–8]. Observations of such landslides reveal a wide range of earthquake related displacements, with surprisingly poor correlation between coseismic and postseismic motion[9]. For instance, the relatively small coseismic displacements (1–2 cm) of the Maca landslide (Peru) were followed by periods of increased velocities for about one month, resulting in three times greater cumulative displacements[10,11]. The Mela-Kabod landslide (Iran), on the other hand, was displaced up to 30 m during the Sarpol-e-Zahab earthquake, with subsequent 5–10 mm postseismic movements over the next three weeks[12]. La Sorbella landslide (Italy), in turn, did not show any measurable increase in activity after coseismic displacements of 0.3–0.8 mm recorded during three earthquakes[13,14]. This large variation in the ratio between coseismic and postseismic motions has also been observed in various landslides affected by the Gorkha earthquake in Nepal[9].

The behaviour of a landslide during seismic shaking is assumed to be mainly governed by inertia and the dynamic stress change in the shear zone[15,16]. Depending on the constitutive properties of the shear zone, the landslide's response can vary from zero to very large displacements. A critical control for a catastrophic coseismic collapse of the slope is the mechanism of strength reduction in the shear zone, such as rate-softening[17,18], grain crushing[19,20] or frictional heating[21]. The coseismic motion of a landslides is further influenced by its geophysical properties, namely the shear wave velocity profile, which could lead to an amplification of the seismic signal[15]. It has also been shown that the landslide geometry can strongly influence the coseismic displacements[22,23].

The wide range of different observed time scales suggest that the postseismic activity of landslides can have several underlying mechanisms[9]. At annual scales, both landslide accelerations[24] and increased landslide rates[25] are controlled by the combined effect of earthquakes and precipitation. These observations can be explained by damage to the landslide material due to earthquake shaking in the form of micro- and macrofractures, which increase permeability and generate preferential paths for water infiltration[11]. The closure of these cracks, often referred to as healing, can take from months to several years, making a landslide more susceptible to precipitation driven movements. Another time scale of postseismic landslide activity, observed in different studies[9–12], ranges from weeks to months. In contrast to the annual scale, this acceleration was observed even in the absence of rainfall, which is why another underlying mechanism is suspected. In a recent study, it was suggested that excess pore water pressures (PWP) are generated outside of the shear zone during seismic shaking and later migrate into this zone by seepage, causing an acceleration of the landslide motion[9]. Depending on the origin of the excess pore water pressures and the soil permeability, this could lead to a time-lag of up to several days between the earthquake and the increased landslide mobility and therefore provides a possible reason for delayed landslide failures[2,26,27]. Although this hypothesis seems to be conceptually reasonable, it has been lacking so far both direct measurements and a quantifiable model for its validation.

According to the fundamental concept of critical state soil mechanics[28], soils that are continuously sheared will come to the so-called critical state. This state is often described as continuous flow at which the volume and porosity of the soils stay constant with increasing shear deformation[29]. Shear zones that have experienced a long history of localized shearing are assumed to have reached this critical state and no or only negligible excess

pressures will be generated during further shearing[30–32]. Hence, a seismic event cannot lead to a direct weakening of the material in such shear zone. However, layers of fine-grained soils of relatively low permeability can be often found around or close to the shear zone of active landslides[4,33,34]. Under cyclic loading (e.g., earthquake shaking) these soils show a strong contractive behaviour if the initial void radio is larger than the critical state void ratio[35,36]. During the fast process of earthquake shaking in saturated soils, this contraction is impeded because the water cannot be displaced from the pores fast enough. This leads to generation of excess PWP, which means a reduction in effective stresses. For large cyclic stress amplitudes and loosely packed, water-saturated soils, the effective stresses can reduce close to zero causing the well-known phenomena of cyclic liquefaction[35]. Although this phenomena of seismic liquefaction is mostly relevant for the coseismic triggering of debris flows[37], the behaviour of active landslides can already be influenced by relatively small reduction in effective stresses[38], caused by lower excess PWP, which can migrate into the shear zone and perturb the quasi-static state of the landslide.

In this paper, we propose a dynamic hydro-mechanical model to study the generation of excess PWP during earthquake shaking and the following diffusion process. This model combines the well-known mechanism of generation of excess PWP as a result of cyclic shearing during an earthquake[35] and the rate-dependent behaviour of shear zones[17]. By applying it to parametric and case studies, we attempt to understand the underlying mechanism and to assess the plausibility of the hypothesis that excess PWP, generated outside of the slip surface, can be the main source of post-seismic landslide activity. This will also provide an insight into why the observed coseismic and postseismic landslide movements are so poorly correlated.

Results

Landslide model. In order to investigate the hydro-mechanical behaviour of active landslides during earthquakes, we propose a simplified model assuming infinite slope conditions (Fig. 1). The landslide is reduced to slope parallel layers including a base, stable soil and landslide mass, where the latter are separated by the shear zone (slip surfaces). The local stratigraphy can be accurately represented by splitting the soil above and below the shear zone into a number of sublayers with different constitutive models and parameters. The landslide model is based on the theory of saturated porous solids und dynamic conditions introduced by Biot[39,40], which is solved using a finite element discretization. This represents a unified framework, where the mechanism of seismic wave propagation, landslide movements and PWP dissipation are included. However, to get an accurate representation of the landslide behaviour it is crucial to select appropriate constitutive models for the shear zone and the adjacent soil.

The shear zone is assumed to have experienced a long history of localized shearing and therefore remains in the critical state, where no or only negligible excess pressure will be generated[30–32] during seismic loading. To model shearing rates over several orders of magnitudes during the pre-, co- and postseismic periods of landslide evolution, a conventional logarithmic rate-hardening friction law is used for the shear zone[41–43]. The corresponding relationship between the friction coefficient μ and the shearing rate ν and can be written as

$$\mu = \mu_0 \left(1 + A \cdot \ln\left(\frac{\nu}{\nu_0}\right) \right) \qquad (1)$$

where μ_0, A and ν_0 are material parameters.

Adjacent to the shear zone, above and below it, two identical layers of fine-grained soils of relatively low permeability are
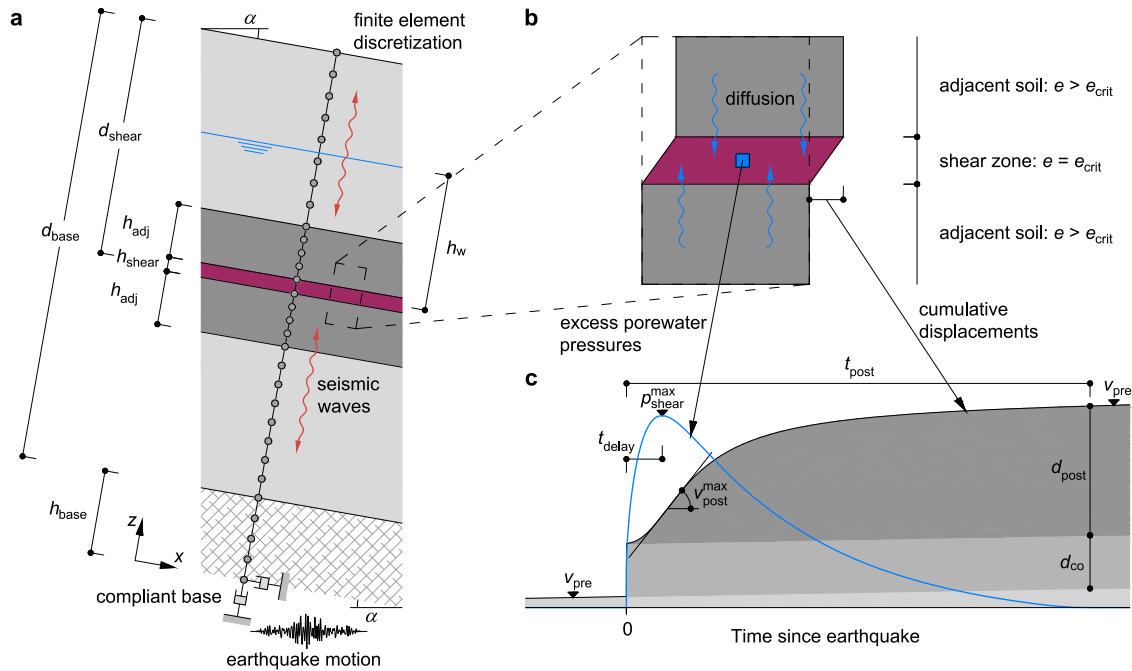
Fig. 1 Landslide model. a The landslide model including the finite element discretization for displacements and pore pressures (considerably more elements are used in the simulations to have a proper representation). **b** Schematic representation of the diffusion of excess pore water pressure from the adjacent soil into the shear zone. The shear zone is assumed to have reached the critical state porosity e_{crit}, whereas the adjacent layers have a higher porosity. **c** Schematic representation of the seismic behaviour of landslides: Starting from an preseismic velocity v_{pre}, the landslide is hit by an earthquake leading to coseismic displacements d_{co}. Excess pore water pressures generated in adjacent soil layers can propagate into the shear zone (blue curve) and lead to a post-seismic activity. Depending on the permeability and the thickness of the layers, this effect can last over a period t_{post} lasting from hours and days to several months. The maximal postseismic velocity v_{max}^{post} is achieved when the excess pore pressures in the shear zone reach the maximal value, which can be delayed by the time t_{delay}, while also depending on the permeability and thickness of the layers.

assumed. As pointed out in the introduction, these soils have not yet reached the critical state and, therefore, can experience an accumulation of excess PWP along with the stiffness and strength degradation[35,36]. Therefore, a multi-surface plasticity model following the framework developed by Prevost[44] is applied in this work. The basic idea is that for each yield surface the volumetric behaviour is defined to control whether the soil shows a contractive or dilative behaviour. In case of undrained cyclic loading during earthquake shaking, this can result in generation of excess PWP depending on the stress amplitudes and number of cycles. It should be emphasized that the adjacent layers can be interpreted either as homogenous or as homogenized sequence of different sublayers, representing soil susceptible to the generation of excess PWP near the shear zone. The shear zone is likely to be less permeable than the adjacent layers due to its compacted state[45]. There is, however, some field evidence showing that it can also be more permeable[46]. In this study they are modelled with the same permeability, which allows for reduction in the number of model parameters. This simplification is justified because the thickness of shear zones, typically ranging from millimeters to decimeters[47–50], is orders of magnitude smaller than that to the adjacent layers. Consequently, the shear zone contribution to seepage is small and not sensitive to its permeability. The stable soil and the landslide mass above the adjacent layers are modelled as linear elastic with a considerably higher permeability and can, therefore, be seen as drainage layers. Whether this corresponds to the actual stratigraphy or whether, for example, this is just a layer of sand or gravel bounding the fine-graded soils is less relevant. Even if there are additional layers susceptible to the generation of excess PWP within the stable soil or the landslide mass, in reality they will hardly influence the shear zone since for landslides of finite lengths the drainage layers will predominantly dissipate excess PWP along the slope.

This model should be seen as a generalization of typical landslide conditions[4,33,49,51] to investigate the underlying mechanism. More details on the landslide model, the applied constitutive models and the corresponding parameters are presented in the Methods section.

Conceptual model response. The conceptual response of the proposed model and some fundamental mechanisms are explained in Fig. 2. The initial state of the model is given by the quasi-static equilibrium, where the landslide is slowly moving at the preseismic velocity v_{pre} sufficient to counterbalance driving forces by the rate-dependent shear strength. If this model is subjected to an earthquake ground motion, the shear zone and the adjacent soil will show different responses, which in cases of low permeability do not interfere with each other. The seismic shear stress amplitude can occasionally exceed the strength of the shear zone leading to a temporary stepwise acceleration of the landslide. Due to the large scale of the horizontal axis in Fig. 1c, these steps are indistinguishable and show up as a single step of coseismic displacement d_{co}. The increase in velocity will simultaneously mobilize a higher shear strength according to the logarithmic rate-dependency and counteract the acceleration to some extent. Consequently, smaller coseismic displacements are expected for a higher rate-dependency parameter A. Since the shear zone remains at critical state, no excess PWP are generated in it and the effective normal stress stays constant during seismic shaking. This is illustrated by the vertical coseismic effective stress-path in Fig. 2a. In contrast, in the adjacent layers excess PWP are generated during cyclic shaking, which is shown by the reduction in effective stresses in Fig. 2b. While for a high permeability, the response of the shear zone and the adjacent soil
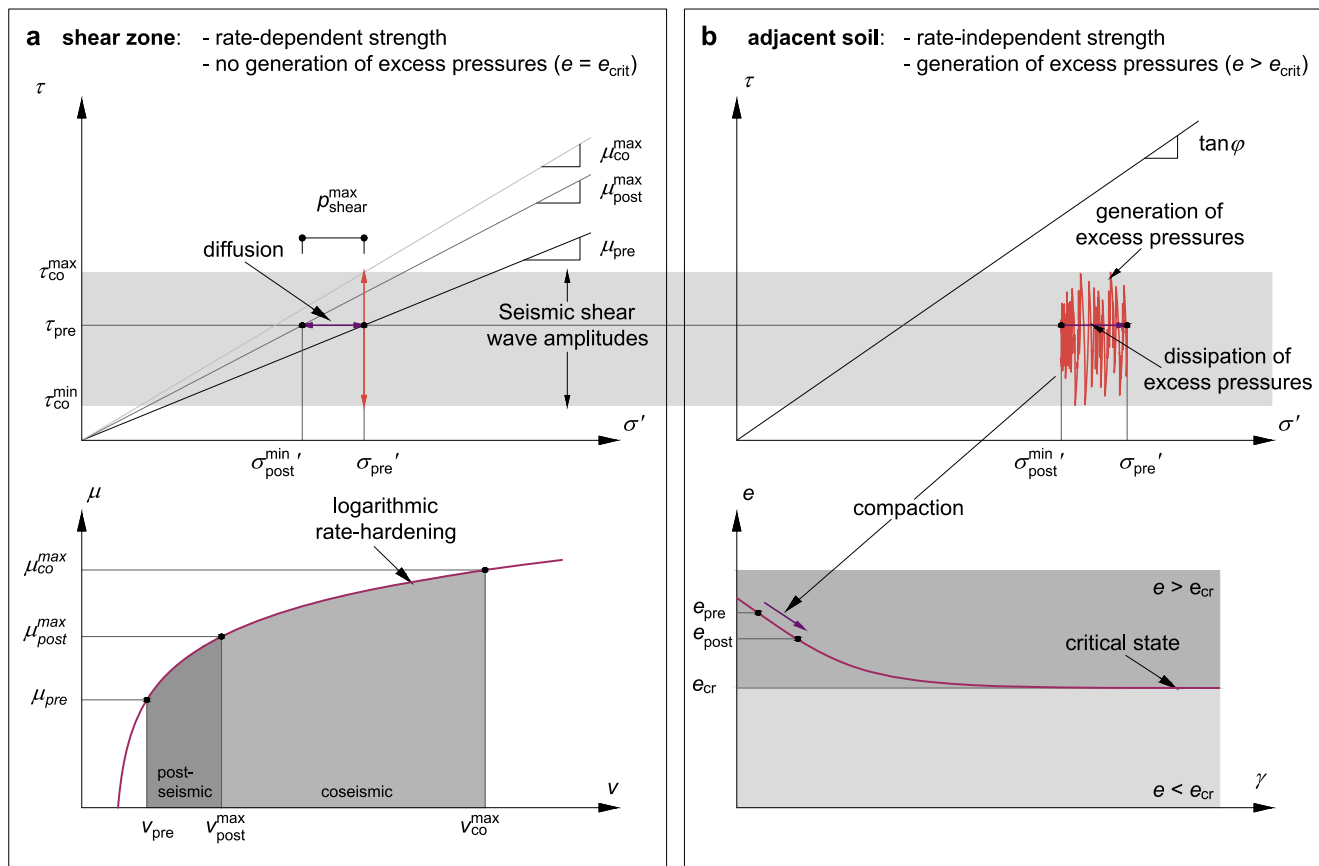
Fig. 2 Conceptual model response. a Stress-path in the space of effectiv normal stress σ' and shear stress τ and rate-dependent friction law inside the shear zone. During the seismic shaking, no excess pressures as generated and a higher friction can be mobilized due to the increased coseismic velocity. After the earthquake the diffusion of excess PWP into the shear zone leads to a reduction of the normal effective stress until the minimal value σ'^{min}_{post}. This reduction in effective stress leads to a reduction in the shear resistance accelerating the landslides to a maximal postseismic velocity v^{max}_{post}. Therefore, the reduction in the shear resistance is counterbalanced by the rate dependency leading to a new quasi-static state. During the further diffusion process, the landslide is continuously decelerated to the preseismic velocity v_{pre}. **b** Stress-path and compaction in the adjacent soil layers. The cyclic shaking with maximal and minimal shear stress amplitudes of τ^{max}_{co} and τ^{min}_{co} leads to a generation of excess PWP shown by reduction in the effective normal stress from σ'_{pre} to σ'^{min}_{post}. During the following postseismic dissipation process the soil in the adjacent layers starts to compact shown by the reduction of the void radio from e_{pre} to e_{pos}.

cannot be separated and they interfere with each other, the hydro-mechanically coupled dynamic approach used here correctly handles this interaction.

After the earthquake, the diffusion process will start and continue over a longer time scale. The excess PWP in the adjacent layers will propagate into the layers above and below as well as into the shear zone, where this reduction of the effective stress causes a drop in shear strength, resulting in landslide acceleration. Due to the rate dependency of strength, however, this acceleration will cause an increase in strength, compensating for the reduction in effective stresses and allowing the landslide to find a new equilibrium, but at a higher velocity. It follows, that for the same excess PWPs, the higher is the rate dependency, the lower will be the new elevated velocity. As the PWPs gradually dissipate after the earthquake, a progressively smaller velocity will be sufficient to compensate for the strength drop, until all the excess PWP fully dissipate and the landslide returns to its preseismic velocity.

Simulation example. The first simulation of an example case, based on the Maca landslide[33] and the typical range of parameters (e.g., thickness, slope inclination, landslide velocity)[4], aims to show the capability of the presented model and reveals effects of different phenomena on the seismic acceleration of landslides. The applied parameters are presented in Table 1 in the methods

section. Rather different patterns can be observed for pre-, co- and postseismic displacements (Fig. 3a). The initial state of slow movements is interrupted by a short period of distinct displacement steps induced by the earthquake impulses (Fig. 3b), which is similar to the results from a traditional Newmark's sliding block analysis[16]. After the earthquake, the landslide shows a one day-long acceleration followed by a deceleration over several days reverting to the pre-seismic velocity. The generation of excess PWP in the adjacent soil layers during the earthquake and the following diffusion into the shear zone are presented in Fig. 3c, d, respectively. The spatial distribution of excess PWP provides several important insights: (a) generation of excess PWP is considerably reduced in the vicinity of the shear zone due to the smaller amplitude of shear stresses, limited by the residual shear strength in the shear zone; (b) since no excess pressures are generated in the shear zone, the only source of their increase is the diffusion from the adjacent soil; (c) the maximal excess PWP reached inside the shear zone is considerably smaller than those in the adjacent soil. The excess PWP in the adjacent soil and the corresponding degradation of strength could theoretically lead to the formation of new shear zones. While the proposed mechanism can capture this effect automatically via the strain softening model used for the adjacent soil, it has not been observed in simulations due to the large difference between the residual

Table 1 Parameters used for the simulations.

| Parameter	Symbol	Demo	Study 1 (Fig. 4)	Study 2 (Fig. 5)	Maca
Geometry					
Inclination	α		12°		
Base thickness	h_{base}		10 m		
Base depth	d_{base}		100 m		
Shear zone depth	d_{shear}		40 m		
Adjacent soil thickness	$h_{adj} = h$	10 m	var.	20 m	30 m
Shear zone thickness	h_{shear}		0.1 m		
Water table height	h_w		30 m		
Mechanical parameters					
P-wave modulus base	M_{base}		15 GPa		
S-wave modulus base	G_{base}		5 GPa		
Density base	ρ_{base}		2700 kg m^{-3}		
P-wave modulus soil[77]	M_{soil}		320 MPa $\cdot(\sigma_0/100$ kPa$)^{0.5}$		
S-wave modulus soil[77]	G_{soil}		80 MPa $\cdot(\sigma_0/100$ kPa$)^{0.5}$		
Density soil	ρ_{soil}		2000 kg m^{-3}		
Permeability					
Permeability base	k_{base}		10^{-6} m s^{-1}		
Permeability stable soil and top soil	k_{soil}		10^{-6} m s^{-1}		
Permeability shear zone and adjacent soil	k	0.5·10^{-8} m s^{-1}	var.	10^{-8} m s^{-1}	0.5·10^{-8} m s^{-1}
Shear zone					
Reference velocity	v_0	1.0 cm y^{-1}	0.1 m y^{-1}	0.1 m y^{-1}	3.1 cm y^{-1}
Rate dependency parameter	A	0.01	var.	0.01	0.0043
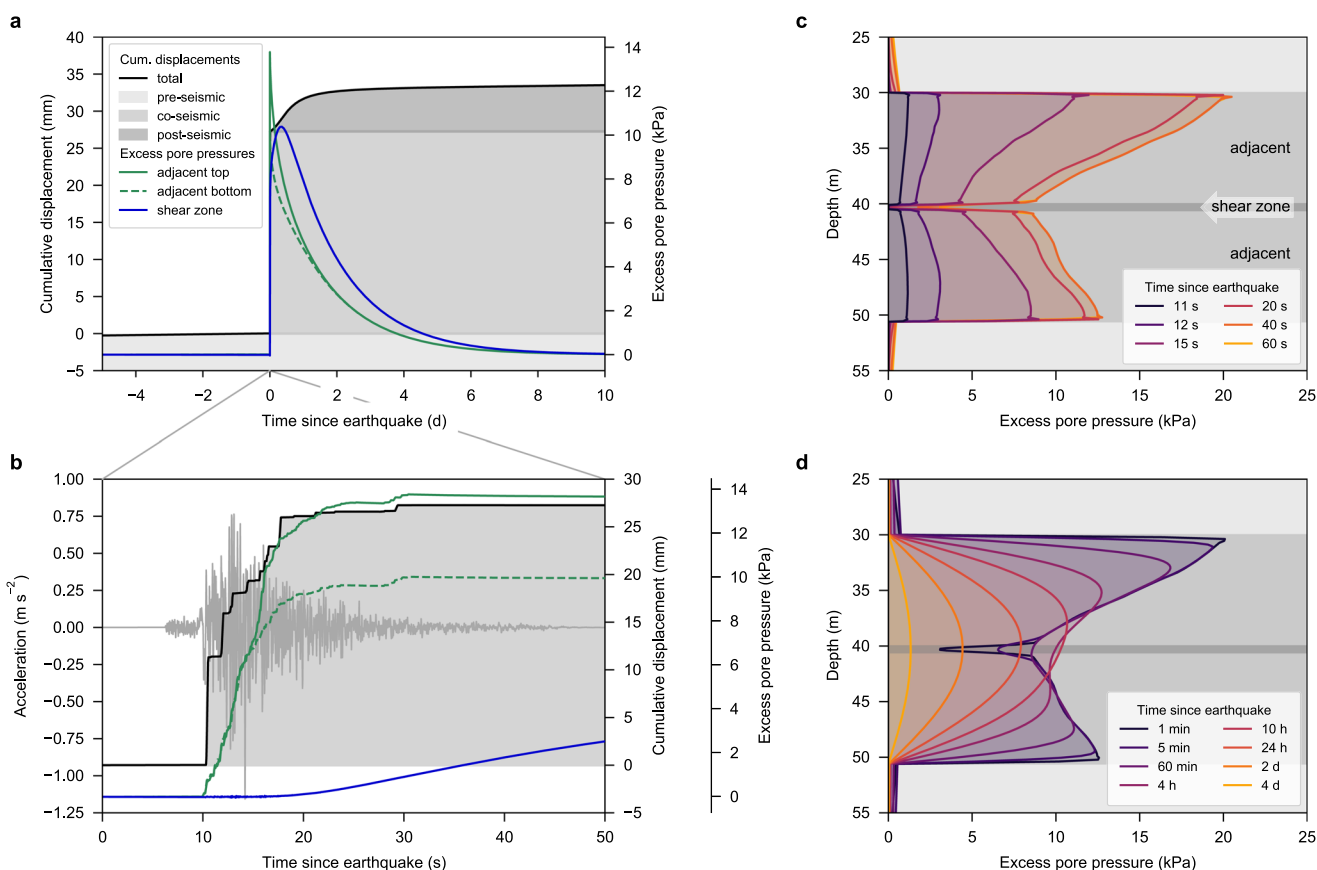
Fig. 3 Example simulation. a Cumulative displacements split into pre-, co- and postseismic contributions and the evolution of excess pore water pressures in the shear zone and the adjacent layers (average). **b** Zoom of the co-seismic behaviour showing the input ground motion (Engineering Strong Motion (ESM) database signal ID: IT-MNF-EMSC-20161030_0000029-HE[56]), cumulative displacements and the evolution of excess pore water pressures in the shear zone and the adjacent layers. **c** Generation of excess pore water pressures in the adjacent soil layers during the earthquake (shear zone marked in dark grey). **d** Dissipation of excess pore water pressures during the postseismic period (shear zone marked in dark grey).

strength of the shear zone and the peak strength of the adjacent soil. If the shear zone and the adjacent layers are identical soils of low clay content, these strengths are closer together since the phenomena of particle reorientation leading to a low residual strength[30] is less dominant. In such a scenario, however, the adjacent layers would be already close to fully mobilized strength and the critical state. Therefore, the excess PWP generated during an earthquake cannot be substantial, making a postseismic acceleration less likely.

The initial increase and the following dissipation of excess pressures in the shear zone explain the observed post-seismic landslide acceleration and deceleration due to the associated reduction of effective stresses and hence change in the shear resistance. While the geometry, material parameters and seismic loading chosen for this demonstration example are realistic and produce a possible co- and post-seismic slope behaviour, this alone does not provide an insight into relative effects of individual parameters and corresponding mechanisms.

Interplay between rate dependency and excess PWP. The parametric study in Fig. 4. investigates the influence of the most important factors and assesses the potential patterns of between coseismic and postseismic landslide activity. The basis for this simulations is again the Maca landslide[33] with the ranges for landslide parameters given in Lacroix et al.[4]. It is important to recognize the analogy between the dissipation of excess PWP from the adjacent soil and the one-dimensional consolidation theory[52], which describes the consolidation process in soils where only unidirectional seepage flow is taking place. A key finding of this theory is that the time until a certain percentage of the excess PWP is dissipated is proportional to the characteristic consolidation time $T = k\gamma_w/(h^2 M)$. Applying this concept to the dissipation of excess PWP in the adjacent layers, the results are plotted with respect to this characteristic time, where $h = h_{adj}$ is the thickness, k the permeability; M the average constrained modulus of the adjacent layers and γ_w is the specific weight of water. The linear dependency of the duration of postseismic motion on the characteristic time (Fig. 4a) confirms the consolidation analogy. Therefore, the characteristic time can be interpreted as an important landslide-specific parameter, uniquely defining the postseismic duration, regardless of the rate-dependent characteristics of the shear zone material or earthquake intensity. The latter finding is confirmed by observations of the Maca landslide, where two earthquakes of different intensities resulted in almost identical postseismic durations[9]. The chosen range of permeability is typical for fine-grained soils found in landslides[50,53,54]. For more clayey layers, a smaller permeability is locally possible, but the comparison of lab and field tests has shown[45] that the field permeability is usually larger due to in homogeneities. It is rather questionable whether a homogeneous clayey layer of 30 m thickness with a permeability of $k = 10^{-10}$ m s^{-1} can be encountered in a real landslide. However, thinner layers with such a permeability are indeed realistic[45,46], and can lead to postseismic movements over a period of several years.

The coseismic displacements (Fig. 4b) are mainly governed by the rate dependency of the shear strength in the shear zone and can vary over several orders of magnitudes for a typical range of observed rate dependencies[17]. In contrast, the postseismic displacement (Fig. 4c) is controlled by both the rate dependency and the characteristic time. Dependency on the characteristic time (i.e., duration) is straightforward, because for the same postseismic velocity, a longer duration naturally leads to a larger postseismic displacement. The effects of rate dependency of strength are, however, more complicated. As expected, the postseismic displacement grows with the maximal postseismic landslide velocity, which in turn increases with the maximal

excess PWP in the shear zone. The complication arises from the fact that rate dependency has two opposite effects on the pore pressures and the velocity. While on one hand, similar to the preseismic state, a higher rate dependency of the shear zone leads to a lower postseismic velocity (Fig. 4d); on the other hand it results in higher coseismic excess PWP (Fig. 4e). The latter can be explained by the isolating effect of the shear zone, which for a low rate dependency can sustain and transfer only limited shear stress amplitudes, resulting in lower excess PWP in the adjacent layers. For higher rate dependency, however, this isolating effect becomes less prominent, because the shear zone behavior remains practically elastic, transferring shear waves of higher amplitudes and causing higher excess PWPs. These counteracting effects of rate dependency can be separated by using the ratio between the maximal postseismic velocity and excess PWP (Fig. 4f), which can be interpreted as a pressure-normalized postseismic velocity. This establishes rate dependency as the main influencing factor for both the velocity and PWP, and highlights the decoupled nature of the two different time-dependent mechanisms affecting the postseismic acceleration: consolidation/seepage (affecting duration) and rate dependency (affecting velocity/ PWP) and their relative contributions to the post-seismic displacements. Unravelling this elegant interplay between rate dependency and excess PWP has been critical for understanding the between coseismic and postseismic landslide behaviour. This understanding would, however, be incomplete without an insight into effects of another critical factor – seismic loading.

Influence of earthquake intensity vs the field evidence. The influence of the earthquake intensity on the landslide activity has been investigated by subjecting the landslide model to a large set of variable input signals. The comparison of the results with the measurements from different case studies[9–12,14,24] is presented in Fig. 5. Amongst the most popular intensity measures the peak ground velocity (PGV) was found to provide the best correlation between coseismic and postseismic landslide activity and the earthquake intensity. The postseismic motion is plotted as a displacement ratio, where the post-seismic displacement is normalized by a yearly reference displacement resulting from a constant preseismic velocity. In the preseismic state, the equilibrium is maintained because the reduction in shear resistance caused by a precipitation-driven increase in PWP is counterbalanced by rate-hardening of the shear zone due to an increased landslide velocity. The postseismic motion can be viewed as a perturbation of the preseismic state by a coseismic increase in PWP, suggesting that the postseismic landslide velocity should directly correlate with the preseismic velocity, as confirmed by a parametric study in Supplementary Fig. 1. Additionally, the comparison of the results shown in Fig. 5 is provided in non-normalized form in Supplementary Fig. 2.

Both coseismic and postseismic displacements clearly increase with increasing ground motion intensity, where the fastest logarithmic increase takes place at lowest intensities and a saturation can be observed for intensities at PGV > 0.1. This observation can be explained by the isolating effect of the shear zone, hindering the transfer of large amplitude impulsive shear waves from stronger earthquake motions. Although the postseismic displacement ratio shows a larger scatter, it can still be observed that the post-seismic activity decays slightly faster with the decreasing intensity. This trend has already been detected in real landslides[9]. In general, the simulation results are in good agreement with the measurements from the case studies. In cases where no postseismic motion was measured, it is assumed to be within the order of the accuracy of the measurements.
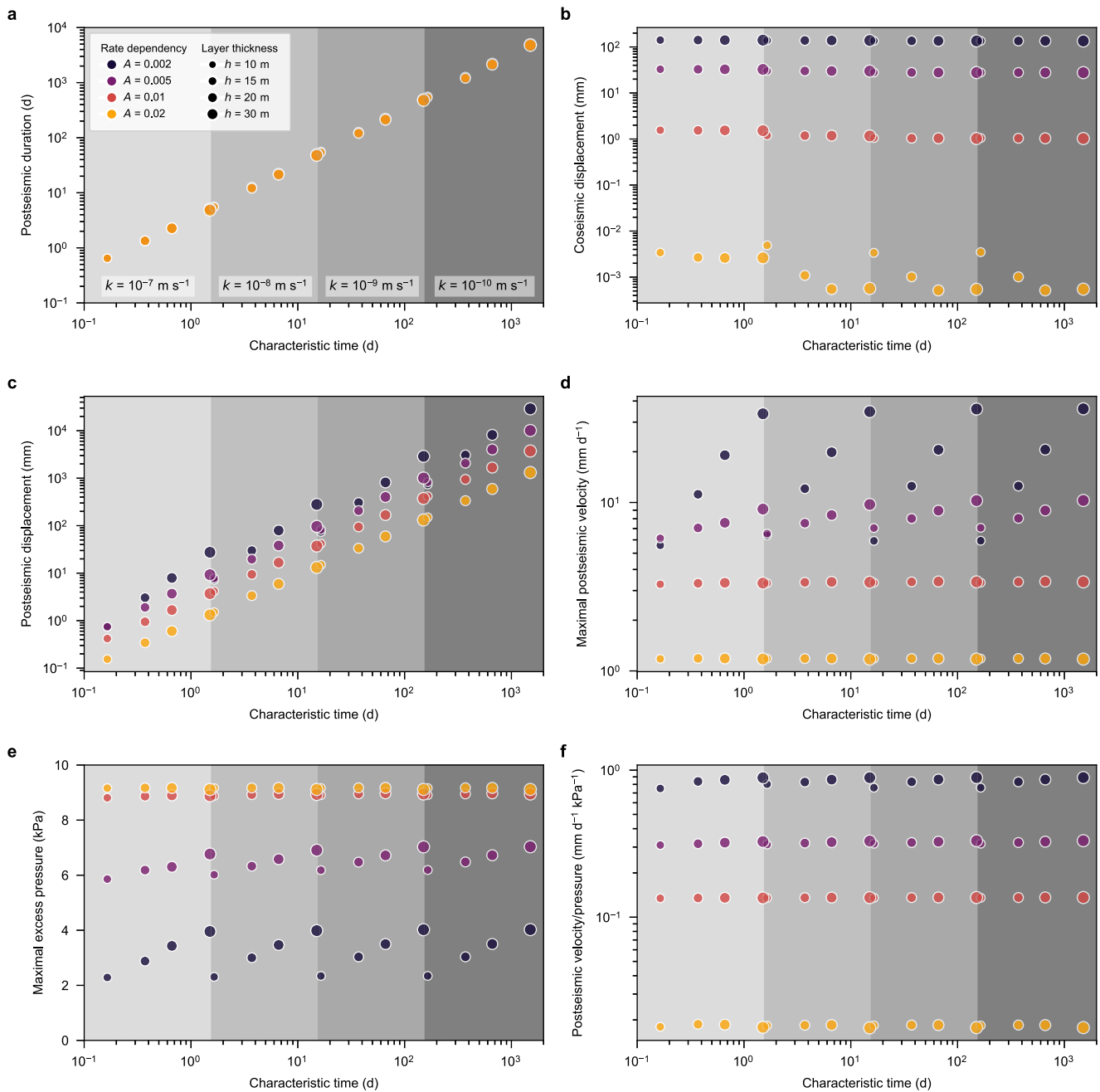
Fig. 4 Parametric study of co- and post-seismic landslide activity. Simulation results showing the influence of the rate dependency of the shear zone (parameter A), thickness of the soil layers adjacent to the shear zone ($h = h_{adj}$) and the permeability of the shear zone and the adjacent soil layers k. The results are plotted on the horizontal axis using the characteristic time $T = k\gamma_w/(h^2 M)$, where γ_w is the specific weight of water and M the average constrained modulus of the adjacent soil layers, for: **a** Duration of the postseismic period of increased landslide activity, starting after the earthquake and ending once 95% of the excess PWP has been dissipated. The markers for different rate dependencies lie exactly on top of each other and are therefore not visible. **b** Coseismic displacements. **c** Postseismic displacement. **d** Maximal postseismic velocity. **e** Maximal excess pore pressure inside the shear zone. **f** Ratio of the maximal postseismic velocity and the maximal excess pressure. The earthquake motion was retrieved from the ESM database (ESM signal ID: IT-MNF-EMSC-20161030_0000029-HE[56]). The parameters used for the simulations are presented in Table 1.

In case of La Sorbella landslide only very small coseismic and no postseismic displacement were measured during three moderate earthquakes[13,14]. The latter is not surprising given the direct relation between the preseismic and postseismic velocity and the fact that La Sorbella is very slow moving. The simulation seems to slightly underestimate the coseismic motion, which can be explained by the strong influence of the rate dependency. This is confirmed by the simulation results in Supplementary Fig. 3, where the model parameters are adjusted

for the specific case of La Sorbella slide and the corresponding earthquake signal recorded near the landslide is applied. Firstly, the results suggest a higher rate dependency of the shear zone to accurately match the coseismic displacement, which also means that a smaller postseismic velocity is expected for a given excess pressure. Secondly, the lithology of La Sorbella landslide is different from the proposed landslide model and only shows soil susceptible to excess PWP above the shear zone. This is considered in the case-specific simulation
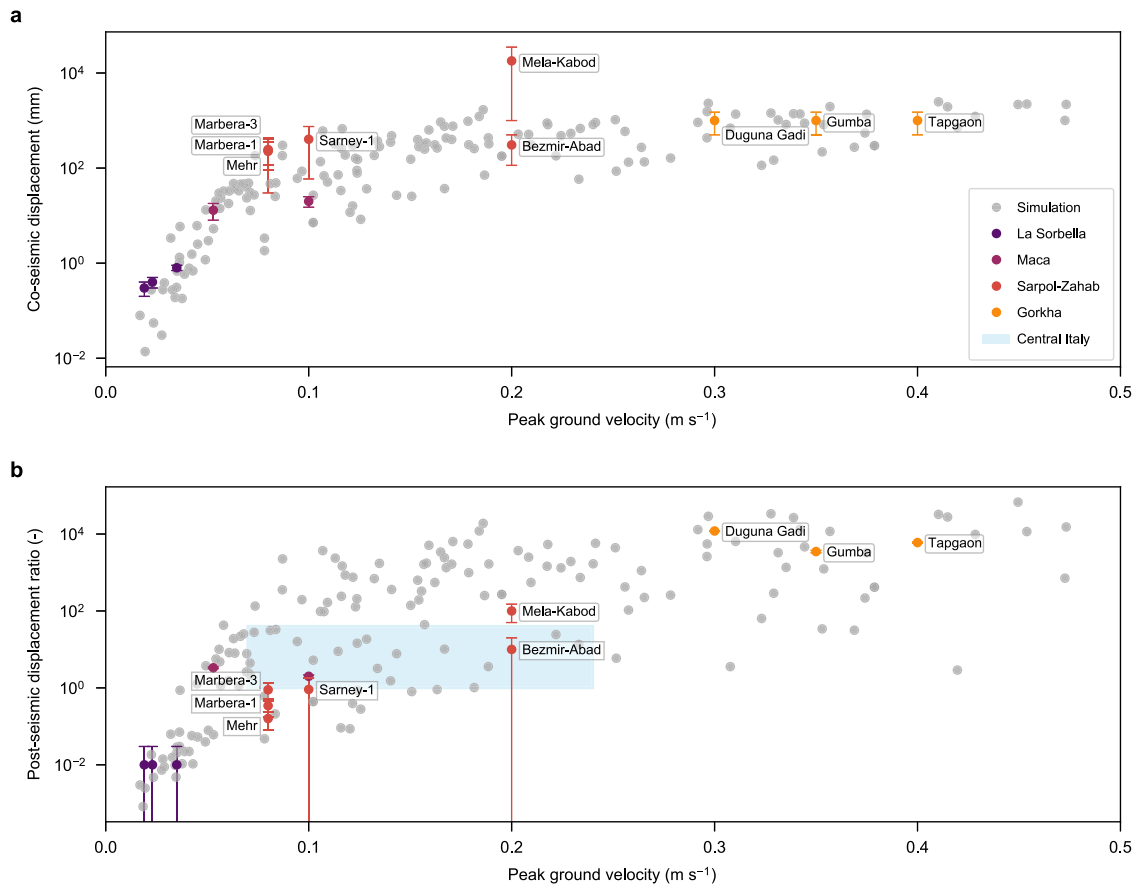
Fig. 5 Influence of the earthquake intensity on the landslide motion. Comparison of simulations to measurements from case studies for a large set of earthquake signals. **a** Coseismic displacements and **b** postseismic displacement ratio given by normalizing the postseismic displacement with a yearly reference displacement resulting from a constant preseismic velocity. The input signals from rock or stiff soil sites were retrieved from the ESM database[56] and are listed in the Supplementary Table 1. The case studies considered are: La Sorbella landslide[14], Maca landslide[10,11], Sarpol-Zahab earthquake[12] (Slides: Marbera-1, Marbera-3, Mehr, Sarney-1, Mela-Kabod, Bezmir-Abad), Gorkha earthquake[9] (Slides: Duguna Gadi, Gumba, Tapgaon) and landslides in Central Italy[24]. The landslides from the Gorkha study show almost no preseismic motion and the reference velocity for the normalization is assumed to be 2 cm/year based on landslide velocity detected in a nearby valley[76]. Error bars represent the measurement error reported in the respective publications. Except for La Sorbella, the input signals are not available and the peak ground acceleration was estimated based on the USGS shakemap (https://earthquake.usgs.gov/data/shakemap/). The parameters used for the simulations are presented in Table 1.

(Supplementary Fig. 3) leading to less excess PWP and faster dissipation, which could further explain the missing postseismic movements.

The landslides observed in connection with the Sarpol Zahab earthquake in Iran are described as deep-seated sliding mass of limestone blocks, entrained within clayey and debris material[12]. They are all considered pre-existing landslides, either dormant or active, with velocities ranging from 0 to 43 mm/year. All of them showed clear coseismic displacements, which in general lie within the simulated range, except for the Mela-Kabod slide, where a displacement of around 30 m represents an outlier. Considering the strong influence of the rate dependency (see Fig. 4b), such large displacements could result from a lower rate-hardening. Also other factors decreasing the shear resistance, such as a change from rate-hardening to rate-softening shear behaviour[4], softening in the landslide mass[22] or grain crushing[55] could explain the excessive observed displacements. Some of these landslides (Mela-Kabod, Marbera-1, Marbera 3 and Mehr) showed a postseismic transient motion over 20 days, which fits into the lower range given by the simulation results. Given the insufficient knowledge of the lithology of these slides and that they contain rock as well as soil, they might be less susceptible to excess PWP.

The landslides in Nepal are describe as reactivation of paleo-landslide deposit of breccia material in a silty matrix (Gumba and Duguna Gadi) and a thick rockslide of deformed regolith and weathered bedrock (Tapgaon)[9]. They all share a coseismic displacement of around 1 m, followed by an acceleration during few days after the Gorkha earthquake (with the moment magnitude M_w 7.8) and a similar progressive deceleration for two months. Two interesting observation should be emphasized. Firstly, the Tapgaon slide clearly showed a delay of at least 4 days for the postseismic motion, which may indicate a larger distance between the shear zone and the layers susceptible to generation of excess PWP. Secondly, the Dolakha earthquake (Mw 7.3), an aftershock of the Gorkha event, showed no effect on the postseismic activity of these landslides. An explanation could be that during the strong main shock the contraction potential of the susceptible soil layers has been greatly reduced. Therefore, no or only little PWP were generated during the aftershock.

In a recent study, a large inventory of landslides accelerated by the 2016–2017 Central Italy earthquake sequence was presented[24]. They have reported an average acceleration phase of around one year followed by a stabilization and recovery phase for two years of theses landslides. This falls within the annual time scale of postseismic activity and is usually explained by

different mechanisms[9,11,25]. However, these landslides are still illustrated in Fig. 5 by a shaded area showing their predominant occurrence. Unfortunately, the coseismic displacement of these landslides was not reported and is therefore not shown.

The motion of the Maca landslide[10,11] very well fits the general simulation results, which was expected since this slide formed the basis study case for the proposed model. While this analysis allows for quantifying the main effects of seismic loading on landslide activity, the large range of possible responses to different events of similar intensity is, on its own, an important outcome requiring a better understanding. Towards this goal, the proposed methodology is applied to the Maca landslide in Peru[33] in the following section.

Application to the Maca landslide. Located in a seismically active zone in Peru, the Maca landslide is in a persistent state of slow movements driven by rain and small earthquakes[11]. In 2013, this region was hit by a shallow M_w 6.0 earthquake located 20 km away from the landslide. By means of a permanent GPS station, both the co- and post-seismic displacements could be recorded[10]. Since no appropriate ground motion records are available for this event, the simulation was performed using four different accelerogramms (for rock or stiff soil sites) from earthquakes in other locations (Umbria, Central Italy, Attica, Visso) with similar magnitudes, epicentral distances and PGVs (Fig. 6). The earthquake signals were retrieved from the Engineering Strong Motion (ESM) database[56]. The GPS measurements indicate a post-seismic period of around 50 days. Based on the direct relationship between post-seismic duration and the characteristic consolidation time, the main unknown - permeability - can be adjusted to accurately match the observed duration. The Attica event provides the best fit and is, therefore, used to determine the rate dependency by matching the coseismic displacements. The same rate-hardening parameter is then used for all four input signals to investigate the variability of the landslide behaviour. The results highlight the strong influence of the input motion, which was already observed in Fig. 5. Whereas the Umbria and Attica events give almost identical coseismic displacements, they generate considerably different pore water pressures, leading to different postseismic accelerations. On the other hand, the Attica and Central Italy records produce quite different coseismic displacements but almost identical pore water pressures and postseismic displacements. These findings might explain why a weaker earthquake led to larger postseismic displacements for the Maca landslide[11], likely enhanced by a higher preseismic velocity prior to the weaker earthquake.

It can also be noted that the simulation predicts an acceleration of the landslide over several days, whereas this is not evident in the measured data. However, this acceleration is extremely small in the simulation for the Attica event and is hardly visible. The duration of this acceleration depends in particular on the thickness of the shear zone, and for a thinner zone, this effect would disappear.

It follows that for a hydrologically sensitive landslide, seismic events of similar intensity can produce different (albeit relatively modest) excess PWP resulting in a wide range of postseismic displacements. This variation is due to other earthquake characteristics, but no direct correlation or simple explanation could be identified. Most likely, this is a result of various effects interfering with each other and goes beyond the scope of this work. As expected, the corresponding variation in coseismic displacements is less prominent because it is mainly controlled by rate dependency. This explains the different magnitude of scatter in Fig. 5a, b, and provides additional insight into the

observed lack of correlation between coseismic and postseismic displacements.

Discussion

We proposed a hydro-mechanically coupled finite element landslide model with appropriate constitutive models for shear zones and fine-grained soils under cyclic loading. This allowed us to investigate the potential generation of excess PWP during earthquake shaking and the following diffusion process suggested in various studies as the source of postseismic landslide activity[4,9,11,25,57]. In this study, we provide a hydro-mechanical model in support of this hypothesis and show that, for a reasonable choice of parameters, the often-observed postseismic landslide activity can be explained both qualitatively and quantitatively, in spite of the large variation in observed displacements and apparent lack of correlation between their co- and postseismic components. In an in-depth parametric study, we investigate the underlying mechanisms and identify the most important factors controlling both the coseismic and postseismic motion, which are summarized schematically in Fig. 7.

The comparison with field observation clearly shows that this model can represent the realistic behaviour of active landslides during and after an earthquake. In fact, for the well-documented Maca landslide the model can accurately reproduce the observed evolution of the postseismic motion. A similar trend was also reported for the landslides in Nepal in the weeks following the Gorkha earthquake[9], which supports the proposed model. However, for a better assessment and validation, more information about the geology and hydrology of the slides in Nepal and Iran is necessary. The presented model can be adapted to various conditions and therefore, the simplified assumptions of a shear zone and the adjacent layers should be seen as a generalization in order to investigate the controlling mechanisms.

The presented model can also explain the observed phenomena of delayed landslides response, which has been mentioned for the Tapgaon slide in Nepal[9], but has also been observed for other landslide[2,26,27]. In case of low permeability, the excess PWP developed in the adjacent layers slowly propagates to the shear zone, leading to a delay and a following phase during which the landslide accelerates to the maximal postseismic velocity. This has been shown qualitatively in Fig. 1 and is somewhat evident in two of the Maca landslide simulations (Fig. 6a). A longer delay can be expected for a thicker or less permeable shear zone or an additional layer in between the shear zone and the adjacent layer, which is not susceptible for generating excess PWP and simply elongated the propagation distance.

The increased landslide activity over several years after the Central Italy earthquake[24] is typically attributed to the annual time scale, where other mechanisms are discussed. However, the long-term postseismic duration of several years for less permeable soils, which was shown by the parametric study (Fig. 4), suggests a possibility of the same mechanism of excess PWP generation. This is supported by the fact that these landslides show the dominant lithology of sandstones and claystones[24], which are likely to be heavily sheared and fractured around the shear zone and therefore could be susceptible to generating excess PWP. A major finding of this study is that landslides covering a larger area are more likely to accelerate after an earthquake than smaller ones. In the context of the presented model, one can argue that larger landslides are likely to be deeper seated and therefore consist of thicker layers susceptible to generating excess PWP. The same trend has been reported for the size and the runout of the landside and is assumed to be also controlled by pore water pressures[58]. In addition, smaller landslides are more prone to boundary effects, such as a faster dissipation of excess
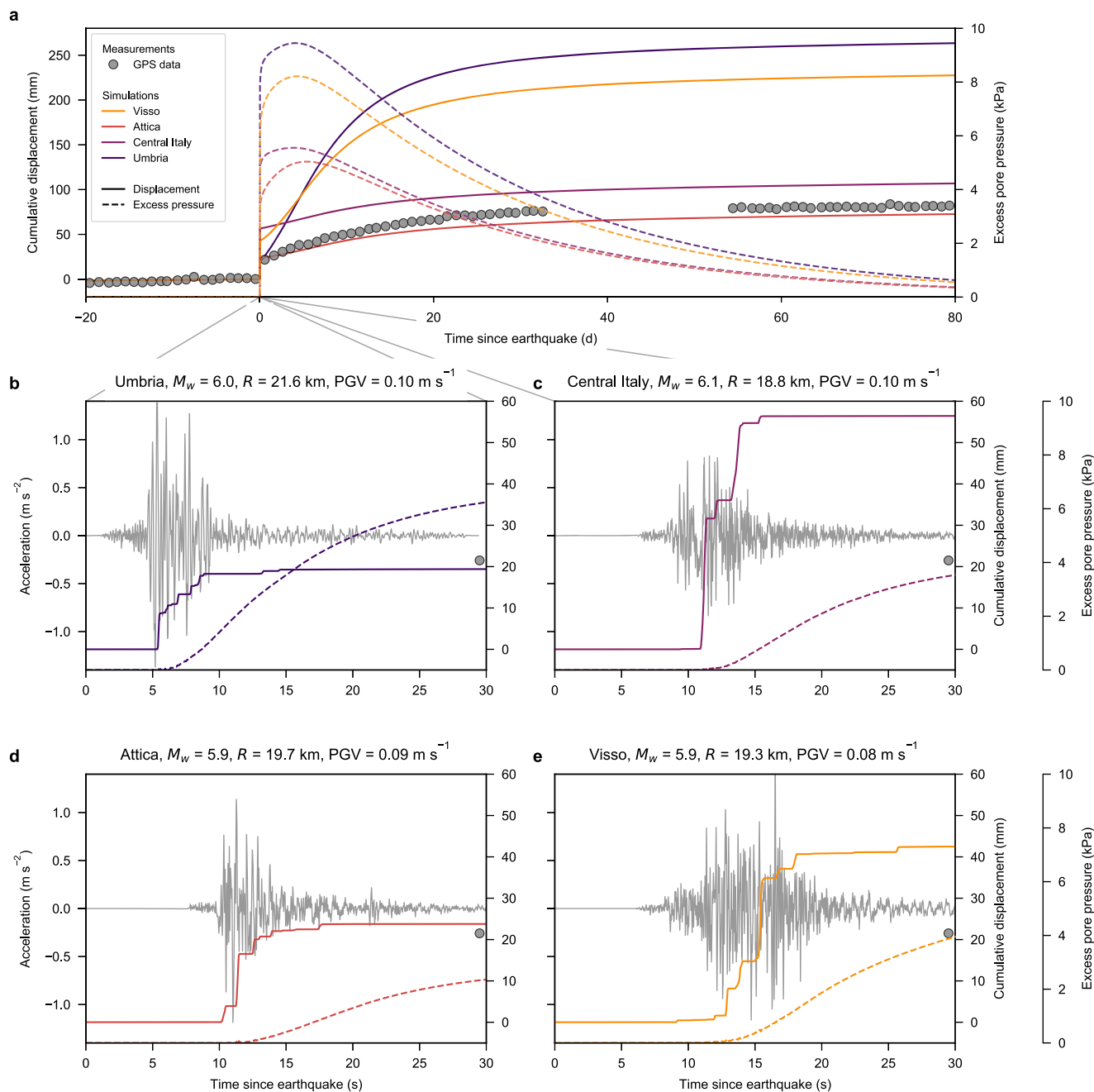
Fig. 6 Application to the Maca landslide in Peru. a Comparison of the GPS measurements (adapted from ref. [10]) and the simulation results for the Maca landslide in Peru. **b**–**e** Zoom into the behaviour during earthquake shaking showing the input ground motion, cumulative displacements and the evolution of excess pore water pressures in the shear zone. The simulation was performed for 4 ground motion signals (rock or stiff soil sites) from earthquakes with similar magnitudes M_w, epicentral distances R and PGVs and were retrieved from the ESM database[56]. The parameters and geometry are based on the morphology of the landslide[33] and are presented in Table 1. The permeability of the shear zone and the adjacent soil are calibrated to accurately match the duration of the postseismic period shown by the GPS measurements.

PWP in the horizontal direction. To assess whether this scenario is plausible or if this mechanism can at least partially contribute to the observed behaviour, more detailed and specific information on these slides is necessary. Another important factor is the inclination of the landslide, which has not been addressed in this study since a change in slope cannot be performed without simultaneously changing other important parameters. In fact, to keep a steeper landslide in a state of mobile quasi-static equilibrium, a higher friction angle is needed. However, a steeper slide with a higher friction angle occurs in soils with higher content of sand and gravel, which usually show lower rate dependency[17].

Therefore, it is difficult to compare different inclinations with each other within the limited scope of this paper, presenting, however, an interesting and important topic for the further research.

The landslide model and the gained insight into the underlying physical mechanisms also provide a possibility to investigate the seasonal response of a landslide. Typically, a strong seasonal dependency in the motion of landslides is observed, which is driven by the effect of rainfall and groundwater changes[11,43,59,60]. The model reaction to a change in the groundwater level could be directly simulated using the proposed model and would even
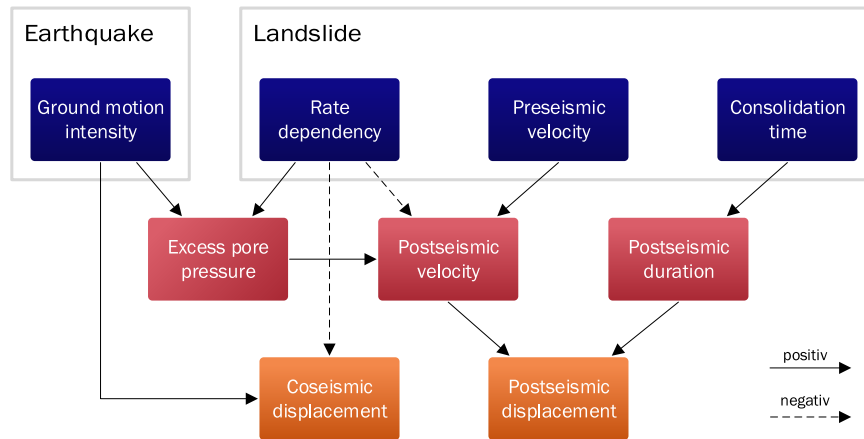
Fig. 7 Schematic representation of the dependencies for coseismic and postseismic motion. Blue: Input quantities/parameters. Red: Intermediate quantities. Orange: Accumulated coseismic and postseismic displacements. Relations, where an increase of the first parameter/quantity leads to an increase of the second, are marked with a solid line and the opposite with a dashed line.

provide an observation-guided calibration of the model parameters (e.g. rate dependency in the shear zone)[49]. Subjecting the model to earthquake shaking in different seasonal states would then allow for a multi-hazard analysis. Given the identified dependency on the preseismic velocity, the model predicts a larger postseismic velocity and displacement for an earthquake during a more active period of the landslide movements. This is due to the logarithmic rate dependent law applied in the shear zone, where for a larger preseismic velocity, a larger absolute increase in the landslide velocity is necessary to compensate for the same excess PWP in the shear zone. Moreover, this makes a landslide more susceptible to acceleration due to rainfall events after an earthquake, when its velocity is still elevated. This behaviour has been reported in different studies[11,24].

Even though not discussed in detail, several related phenomena can be explained by the generation and diffusion of excess PWP outside of the shear zone: reactivation of existing landslides[2,9], initiation of new landslides during and after an earthquake[12,61]. These phenomena are analogous to the presented simulations with the subtle difference of starting at a stable state before the earthquake. Once a new landslide is initiated due to generated excess PWP, a state of slow-moving can be reached in case of rate-hardening shear zones[17] or other factors increasing the resistance, such as geometrical hardening[22] or dilative behaviour of the shear zone[62,63]. However, if rate dependent shear strength cannot counterbalance the effect of excess pore water pressures or, even worse, if other softening mechanisms, such as a softening shear zone[30,55,64], rate softening[17] or grain crushing[19,20] are caused by intensive shearing, a catastrophic failure could be triggered.

Due to the simplifications of infinite slope conditions, 2- or 3-dimensional effects such as multidirectional flow, geometrical effects (e.g., different behaviour of steeper and flatter parts of the landslide, material accumulation or erosion of the landslide's foot) and landslide runout have not been considered in this study and should be investigated in the future. In addition, the presented methodology should be refined and tested by applying it to further case studies. An ideal measurement setup would be an automated inclinometer (with a high measurement frequency to capture coseismic displacements accurately) in combination with several PWP sensors (close to and around the shear zone). This would allow measuring both the evolution of displacements and PWP during and after an earthquake. Finding a suitable landslide in a seismic active area, installing such a measurement system and capturing a strong enough earthquake, seems, however rather

unlikely. Therefore, this topic can be further investigated indirectly by collecting more displacement data from active landslides in seismically active areas using accurate measurement systems (e.g. GNSS, geodetic, extensometers or inclinometers). The lithology of such landslides should be known in order to be able to choose suitable model parameters. Ideally, an extensive experimental investigation (e.g. cyclic triaxial or simple shear tests) on the soil material from the shear zone and the adjacent layers should be carried out. This would provide an assessment for the potential of generating excess PWP in the adjacent layers. In spite of an acute need for reliable risk assessment, surprisingly few such case studies including a proper site investigation have been reported in the literature. We hope that the proposed physical framework can serve as a basis for future site investigations and field monitoring.

Methods

Coupled FE model for infinite slope conditions. The basis for the presented methodology is the theory of saturated porous solids under dynamic conditions introduced by Biot[39,40]. For earthquake analysis the u-p-formulation provides a convenient approximation where the set of equations is written in terms of the soil skeleton deformation $\boldsymbol{u}$ and the pore water pressure p[65,66]. Assuming infinite slope conditions (Fig. 1), the governing equations can be considerably simplified since only derivatives with respect to the z-coordinate (perpendicular to the slope inclination) must be considered. The conservation of linear momentum is given as (time derivatives are denoted as $\dot{u} = \frac{\partial u}{\partial t}$ and $\ddot{u} = \frac{\partial^2 u}{\partial t^2}$)

$$\frac{\partial \boldsymbol{\sigma}}{\partial z} + \rho \boldsymbol{b} = \rho \ddot{\boldsymbol{u}} \qquad (2)$$

where $\boldsymbol{b}$ is a body force (usually gravity) and ρ the total density. The stress tensor $\boldsymbol{\sigma} = \begin{pmatrix} \sigma \\ \tau \end{pmatrix}$ consists of the normal stress σ and the shear stress τ. The other components of the stress tensors are considered under the assumption of infinite slope condition. The balance of mass is given as

$$\frac{n}{K_w}\dot{p} + \varepsilon - \frac{k}{\rho_w g}\frac{\partial^2 p}{\partial z^2} = 0 \qquad (3)$$

where n is the soil porosity, K_w the bulk modulus of water, k the permeability, ρ_w the water density and g the gravitational acceleration. The volumetric strain rate of the soil skeleton $\dot{\varepsilon}$ results from the strain tensor for infinite slope conditions (plane strain with a vanishing strain in direction of the slope)

$$\varepsilon = \frac{\partial \boldsymbol{u}}{\partial z} = \begin{pmatrix} \varepsilon \\ \gamma \end{pmatrix} \to \dot{\boldsymbol{\varepsilon}} = \frac{\partial \dot{\boldsymbol{u}}}{\partial z} = \begin{pmatrix} \dot{\varepsilon} \\ \dot{\gamma} \end{pmatrix} \qquad (4)$$

The behaviour of the soil skeleton is introduced by any constitutive model which relates any strain ε to the corresponding effective stresses[52]

$$\boldsymbol{\sigma}' = \begin{pmatrix} \sigma' \\ \tau \end{pmatrix} = \boldsymbol{\sigma} - p\begin{pmatrix} 1 \\ 0 \end{pmatrix} \qquad (5)$$

This system of Eqs. (2–5) is solved by applying a fully implicit dynamic finite element method similar to one-dimensional ground response analyses[35]. The

landslide is discretized in finite elements perpendicular to the slope inclination as presented in Fig. 1, which allows the accurate representation of different soil and rock layers. To minimize the problem of instabilities in the finite element solution

of Biot's equations, displacements are approximated with quadratic and pore pressures with linear shape functions[67,68].

Aside from the gravitational body force, the landslide is subjected to a dynamic earthquake input motion. To prevent downwards propagating waves from being reflected back into the model, the concept of a compliant base boundary is applied[69]. Therefore, viscous dashpot elements are connected at the base of the model to absorb outgoing waves[70]. In addition, instead of applying the acceleration time history, the input motion is transformed into a boundary traction in slope parallel direction given by

$$t_s(t) = 2v_{su}(t)\sqrt{\rho G} \qquad (6)$$

where ρ and G are the density and shear modulus of the base material. v_{su} is the particle velocity of the upwards propagating wave, i.e. half the outcrop motion[71]. The parameters used for the different simulations are listed in Tables 1 and 2.

Rate-dependent shear zone. The shear zone is modelled by a rate dependent constitutive model. Based on results from ring shear tests on shear zone material[17,18,72], the following logarithmic law for the friction coefficient μ is applied

$$\mu = \tan\varphi = \tan\varphi_0\left(1 + A \cdot \ln\left(\frac{\dot{\gamma} + \dot{\gamma}_0}{\dot{\gamma}_0}\right)\right) \qquad (7)$$

where φ_0, A and $\dot{\gamma}_0$ are material parameters. This type of relation is often chosen for shear zones in active landslides[41–43,73], but the reference strain rate $\dot{\gamma}_0$ is also added in the numerator to avoid the singularity in the logarithm[22]. The strain rate in the shear zone $\dot{\gamma}$ can be linked to the landslide velocity v for a given shear zone thickness h_{shear} as

$$\dot{\gamma} = \frac{v}{h_{shear}} \qquad (8)$$

Based on a given landslide inclination and a reference velocity $v_0 = \dot{\gamma}_0 h_{shear}$, the associated reference friction angle φ_0 can be calibrated.

Table 2 Parameters used for the simulation of fine grained soils.

| Parameter	Symbol	Value
Elasticity		
Constrained or P-wave modulus	M	$320\,\text{MPa} \cdot (\sigma_0/100\,\text{kPa})^{0.5}$
Shear or S-wave modulus	G	$80\,\text{MPa} \cdot (\sigma_0/100\,\text{kPa})^{0.5}$
Hardening		
Hardening parameter	h_0	10.0
Hardening parameter	b	2.1
Volumetric behaviour		
Contraction parameter	β_c	$-22.0 \cdot \sigma_0/M$
Dilation parameter	β_d	$2.2 \cdot \sigma_0/M$
Threshold coordinate	η_p	0.5
Accumulated plastic volumetric strain at full degradation	ε_f^p	$0.44 \cdot \sigma_0/M$
Contraction degradation factor	ζ_f	2 %
Contraction degradation parameter	c	3.0
Reference contraction potential	$\hat{\varepsilon}_{ref}^p$	$0.24 \cdot \sigma_0/M$
Failure		
Inclination of failure surface	$\mu = \tan\varphi$	0.55
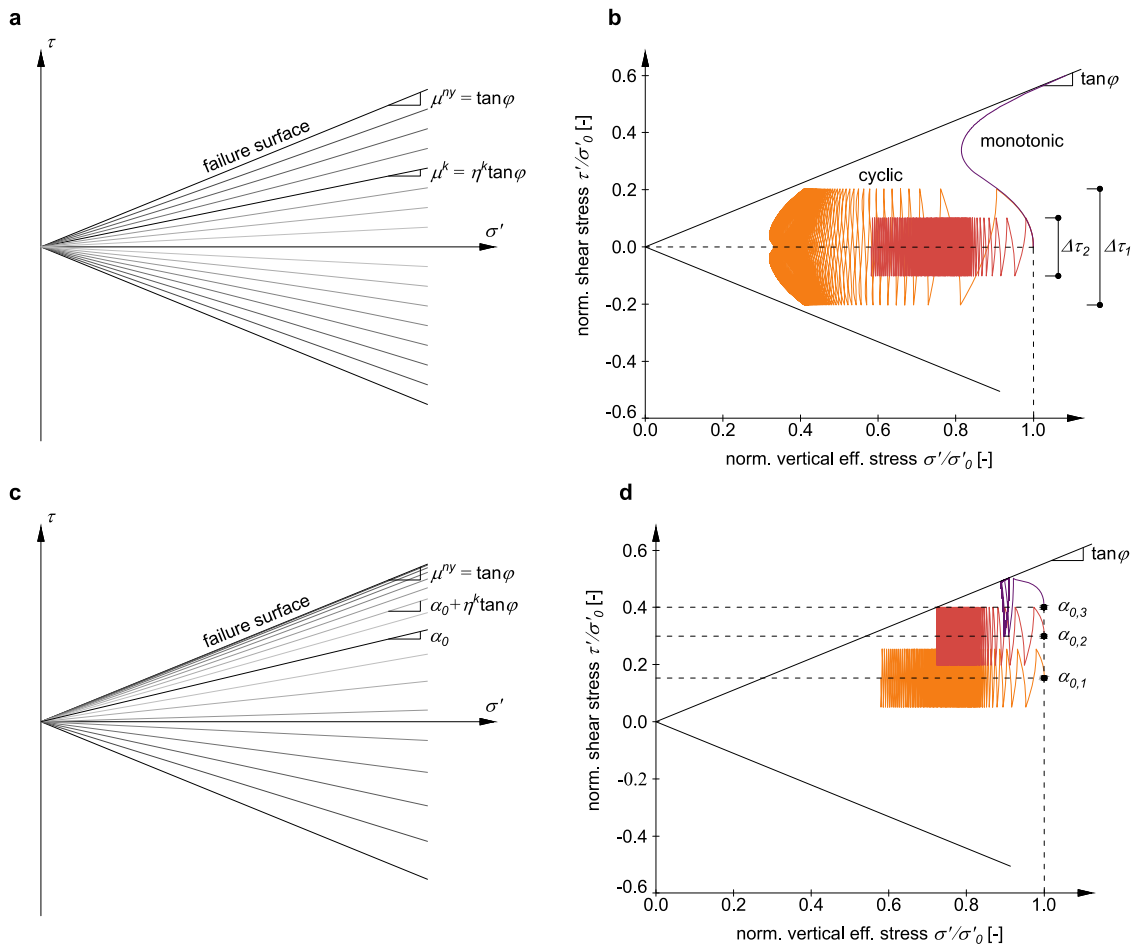
Fig. 8 Constitutive model for cyclic loading of fine-grained soils. a Illustration of the multi-yield surface model. **b** Model response for a monotonic and two cyclic undrained tests with different stress amplitudes (80 cylices). **c** Illustration of the initial arrangement of the yield surfaces after anisotropic consolidation. **d** Model response for cyclic undrained tests for different anisotropic consolidation stresses (80 cycles).

Constitutive model for cyclic loading of fine-grained soils. In this work, the multisurface model developed by Stoecklin et al.[74] is applied. For the integration in the presented numerical framework, the model is simplified by a two-dimensional formulation for the applied infinite landslide conditions, but can easily be transferred to the application of finite slope geometries using the implementation presented by Stoecklin et al.[74]. In the following, the basic equations of the model are presented with an emphasis on the two-dimensional formulation and a slight change in the original formulation also allowing for dilative behaviour. For more details on the model and its implementation the reader is referred to Stoecklin et al.[74].

Based on the general multisurface framework developed by Prevost[44] with n_y-nested yield surfaces $f^1,\dots,f^k,\dots,f^{n_y}$ with frictional, linear, kinematic hardening (Fig. 8a) the yield function for the kth surface has the form

$$f^k = |\tau - \alpha^k \sigma'| - \mu^k \sigma' = 0 \tag{9}$$

where, for a two dimensional formulation, the backstress tensor is reduced to the scalar kinematic hardening variable α^k. The size of the yield surface μ^k is given by

$$\mu^k = \eta^k \mu = \eta^k \tan \varphi \tag{10}$$

where $\mu = \tan \varphi$ defines the failure surface by the friction angle φ. The internal coordinate η^k is linearly spaced between the innermost surface ($\eta^1 > 0$), bounding the elastic region, and the failure surface ($\eta^{n_y} = 1$). Both the volumetric strain rate $\dot{\varepsilon}$ and the shear strain rate $\dot{\gamma}$ are assumed to be decomposable into an elastic and plastic contribution

$$\dot{\varepsilon} = \dot{\varepsilon}^e + \dot{\varepsilon}^p \tag{11}$$

$$\dot{\gamma} = \dot{\gamma}^e + \dot{\gamma}^p \tag{12}$$

where the superscripts e and p denote the elastic and the plastic part. The elastic contribution is described by linear and isotropic elasticity. The normal and shear stresses hence follow as

$$\sigma = M\varepsilon \tag{13}$$

$$\tau = G\gamma \tag{14}$$

where M and G denote the constrained or P-wave modulus and the shear or S-wave modulus respectively. Following the approach by Elgamal et al.[75], the flow rule on each surface has an associative deviatoric and a nonassociative volumetric component

$$\dot{\gamma}^{p,k} = \dot{\lambda}^k \hat{n} \tag{15}$$

$$\dot{\varepsilon}^{p,k} = -\beta^k \dot{\lambda}^k \tag{16}$$

where $\dot{\lambda}^k$ is the plastic multiplier and $\hat{n}$ is equal 1 or −1 for flow at the top or bottom yield surface respectively. The shear-volumetric coupling is controlled by the flow variable β^k, where a negative value results in contractive and a positive in dilative plastic strains on the corresponding yield surface. The total strain increment is given by the sum of the elastic increment and the contribution of all active surfaces

$$\dot{\varepsilon} = \dot{\varepsilon}^e + \sum_k \dot{\varepsilon}^{p,k} = \dot{\varepsilon}^e - \sum_k \beta^k \dot{\lambda}^k \tag{17}$$

$$\dot{\gamma} = \dot{\gamma}^e + \sum_k \dot{\gamma}^{p,k} = \dot{\gamma}^e + \sum_k \dot{\lambda}^k \hat{n} \tag{18}$$

The hardening is governed by a purely deviatoric, linear hardening rule

$$\dot{\alpha}^k = h^k \dot{\lambda}^k \hat{n} \tag{19}$$

where h^k is the hardening modulus. To control the behaviour of the model, both the flow variable β^k and the hardening modulus h^k can be defined for each yield surface independently. The latter is defined according by the hardening function[74]

$$h^k = h_0 n_y (1 - \eta^k)^b \tag{20}$$

where h_0 and b are hardening parameters. The total number of yield surfaces n_y is included to avoid a dependency of the hardening parameters on the chosen number of surfaces. The hardening parameters allow to match the model response to stress-strain curves from simple shear tests or to modulus reduction and material damping curves[74]. The flow variable is defined slightly differently as originally proposed to also account for the dilative behaviour often observed in fine-grained soils

$$\beta^k = \begin{cases} \beta_c \cdot \max\left(\frac{\varepsilon_f^p - \varepsilon^p}{\varepsilon_f^p}, (\zeta_f)^{1/c}\right)^c - \frac{\hat{\varepsilon}^p}{\hat{\varepsilon}_{ref}^p} & \eta^k \le \eta_p \\ \beta_d & \eta^k > \eta_p \end{cases} \tag{21}$$

where $\beta_c < 0$ defines the contraction associated with the initial state of the material for the yield surface with an internal coordinate below η_p and $\beta_d > 0$ controls the dilation for the surfaces above. The dependency on the accumulated plastic

volumetric strain ε^p leads to a diminishing of an initial contraction β_c to residual contraction of $\zeta_f \beta_c$ at the accumulated plastic volumetric strain ε_f^p and can be controlled by parameter c. Additionally, the cyclic contraction potential $\hat{\varepsilon}^p$ is introduced as

$$\hat{\varepsilon}^p = \int_0^t \dot{\alpha}^p dt \text{ with } \dot{\alpha}^p = \begin{cases} \dot{\varepsilon}^p & \text{if } \hat{\varepsilon}^p \ge 0 \\ 0 & \text{else} \end{cases} \tag{22}$$

Hence the cyclic contraction potential grows if the material is dilating and decreases to a minimal value of zero in case of contraction. Including this contraction potential into Eq. 21 results in the butterfly-like shape for undrained cyclic tests and can be controlled by the parameter $\hat{\varepsilon}_{ref}^p$.

Figure 8b shows the model response for a monotonic and two cyclic undrained tests with different stress amplitudes using the parameters presented in Table 2. To take into account the effect of anisotropic consolidation, the yield surfaces are rotated by specifying an initial value of the corresponding hardening variable α_0^k (Fig. 8c), which is often referred to as a "memory" variable[44] and given as

$$\alpha_0^k = \alpha_0 \left(1 - (\eta^k)^{\frac{\tan \varphi}{\alpha_0}}\right) \tag{23}$$

where the consolidation stress ratio is given as $\alpha_0 = \tau_0 / \sigma_0'$. The model response for cyclic undrained tests for different anisotropic consolidation stresses is shown in Fig. 8d using the same parameters presented in Table 2. The same set of parameters are used for all the landslide simulations.

Data availability

Code availability

References

1. Froude, M. J. & Petley, D. N. Global fatal landslide occurrence from 2004 to 2016. *Nat. Hazards Earth Syst. Sci.* **18**, 2161–2181 (2018).
2. Keefer, D. K. Investigating landslides caused by earthquakes - A historical review. *Surv. Geophys.* **23**, 473–510 (2002).
3. Rodríguez, C. E., Bommer, J. J. & Chandler, R. J. Earthquake-induced landslides: 1980-1997. *Soil. Dyn. Earthq. Eng.* **18**, 325–346 (1999).
4. Lacroix, P., Handwerger, A. L. & Bièvre, G. Life and death of slow-moving landslides. *Nat. Rev. Earth Environ.* **1**, 404–419 (2020).
5. Bonzanigo, L., Eberhardt, E. & Loew, S. Long-term investigation of a deep-seated creeping landslide in crystalline rock. Part I. Geological and hydromechanical factors controlling the Campo Vallemaggia landslide. *Can. Geotech. J.* **44**, 1157–1180 (2007).
6. Hendron, A. J. & Patton, F. D. The vaiont slide — A geotechnical analysis based on new geologic observations of the failure surface. *Eng. Geol.* **24**, 475–491 (1987).
7. Salcedo, D. A. Behavior of a landslide prior to inducing a viaduct failure, Caracas–La Guaira highway, Venezuela. *Eng. Geol.* **109**, 16–30 (2009).
8. Puzrin, A. M. & Schmid, A. Evolution of stabilised creeping landslides. *Géotechnique* **62**, 491–501 (2012).
9. Lacroix, P. et al. SAR and optical images correlation illuminates post-seismic landslide motion after the Mw 7.8 Gorkha earthquake (Nepal). *Sci. Rep.* **12**, 1–13 (2022).
10. Lacroix P., Perfettini, H., Taipe, E., & Guillier, B. Coseismic and postseismic motion of a landslide: observations, modelling, and analogy with tectonic faults. *Geophysical Research Letters.* **41**, 6676–6680 https://doi.org/10.1002/2014GL061170 (2014).
11. Bontemps, N., Lacroix, Larose, E., Jara, J. & Taipe, E. Rain and small earthquakes maintain a slow-moving landslide in a persistent critical state. *Nat. Commun.* **11**, 1–10 (2020).
12. Cheaib, A. et al. Landslides induced by the 2017 Mw7.3 Sarpol Zahab earthquake (Iran). *Landslides* **19**, 603–619 (2022).
13. Ferretti, A., Fruzzetti, V.M.E., Ruggeri, & Scarpelli, G. Seismic induced displacements of 'La Sorbella' landslide (Italy)", *International Conference on*

Earthquake Geotechnical Engineering, (2019). [Online]. Available: https://www.issmge.org/publications/publication/seismic-induced-displacements-of-la-sorbella-landslide-italy.

14. Ruggeri, P., Fruzzetti, V. M. E., Ferretti, A. & Scarpelli, G. Seismic and rainfall induced displacements of an existing landslide: Findings from the continuous monitoring. Geosci. 10, 90 (2020).

15. Jibson, R. W. Methods for assessing the stability of slopes during earthquakes-A retrospective. Eng. Geol. 122, 43–50 (2011).

16. Newmark, N. M. Effects of earthquakes on dams and embankments. Géotechnique 15, 139–160 (1965).

17. Tika, T. E., Vaughan, R. & Lemos, L. J. Fast shearing of pre-existing shear zones in soil. Géotechnique 46, 197–233 (1996).

18. Scaringi, G., Hu, W., Xu, Q. & Huang, R. Shear-rate-dependent behavior of clayey bimaterial interfaces at landslide stress levels. Geophys. Res. Lett. 45, 766–777 (2018).

19. Sassa, K., Canuti, & Yin, Y. Landslide science for a safer geoenvironment. 1. (2014).

20. Sadrekarimi, A. & Olson, S. M. Particle damage observed in ring shear tests on sands. Can. Geotech. J. 47, 497–515 (2010).

21. Vardoulakis, I. Catastrophic landslides due to frictional heating of the failure plane. Mech. Cohesive-frictional Mater. 5, 443–467 (2000).

22. Kohler, M. & Puzrin, A. M. Mechanism of Co-Seismic Deformation of the Slow-Moving La Sorbella Landslide in Italy Revealed by MPM Analysis. J. Geophys. Res. Earth Surf. 127, e2022JF006618 (2022).

23. Pinyol, N. M., Di Carluccio, G. & Alonso, E. E. A slow and complex landslide under static and seismic action. Eng. Geol. 297, 106478 (2022).

24. Song, C. et al. Triggering and recovery of earthquake accelerated landslides in Central Italy revealed by satellite radar observations. Nat. Commun. 13, 1–12 (2022).

25. Marc, O., Hovius, N., Meunier, Uchida, T. & Hayashi, S. Transient changes of landslide rates after earthquakes. Geology 43, 883–886 (2015).

26. Jibson, R. W., Prentice, C. S., Borissoff, B. A., Rogozhin, E. A. & Langer, C. J. Some observations of landslides triggered by the 29 April 1991 Racha earthquake, Republic of Georgia. Bull. Seismol. Soc. Am. 84, 963–973 (1994).

27. Agnesi, V. et al. A multidisciplinary approach to the evaluation of the mechanism that triggered the Cerda landslide (Sicily, Italy). Geomorphology 65, 101–116 (2005).

28. Roscoe, K. H., Schofield, A. N. & Wroth, C. P. On the yielding of soils. Geotechnique 8, 22–53 (1958).

29. Schofield, A.N., & Wroth, C.P. Critical state soil mechanics. McGraw-Hill, (1968).

30. Skempton, A. W. Residual strength of clays in landslides, folded strata and the laboratory. Géotechnique 35, 3–18 (1985).

31. Lemos, L.J. Shear Behaviour of Pre-Existing Shear Zones Under Fast Loading. Adv. Geotech. Eng. Skempt. Conf. (2004).

32. Schulz, W. H. & Wang, G. Residual shear strength variability as a primary control on movement of landslides reactivated by earthquake-induced ground motion: Implications for coastal Oregon, U.S. J. Geophys. Res. Earth Surf. 119, 1617–1635 (2014).

33. Zerathe, S. et al. Morphology, structure and kinematics of a rainfall controlled slow-moving Andean landslide, Peru. Earth Surf. Process. Landf. 41, 1477–1493 (2016).

34. P. W. Oberender, "Creeping Constrained Landslides Under Extreme Environmental and Seismic Conditions", ETH Zurich, 2018.

35. S. L. Kramer, Geotechnical Earthquake Engineering, vol: 6. 1996.

36. Boulanger, R. W. & Idriss, I. M. Liquefaction Susceptibility Criteria for Silts and Clays. J. Geotech. Geoenviron. Eng. 132, 1413–1426 (2006). Nov.

37. Islam, N., Hawlader, B., Wang, C. & Soga, K. Large-deformation finite-element modelling of earthquake-induced landslides considering strain-softening behaviour of sensitive clay. Can. Geotech. J. 56, 1003–1018 (2019).

38. Schulz, W. H., Kean, J. W. & Wang, G. Landslide movement in southwest Colorado triggered by atmospheric tides. Nat. Geosci. 2, 863–866 (2009).

39. Biot, M. A. Theory of Propagation of Elastic Waves in a Fluid-Saturated Porous Solid. J. Acoust. Soc. Am. 28, 168–178 (1956).

40. Biot, M. A. Mechanics of deformation and acoustic propagation in porous media. J. Appl. Phys. 33, 1482–1498 (1962).

41. Wedage, A. M. P., Morgenstern, N. R. & Chan, D. H. A strain rate dependent constitutive model for clays at residual strength. Can. Geotech. J. 35, 364–373 (1998).

42. Alonso, E. E., Zervos, A. & Pinyol, N. M. Thermo-poro-mechanical analysis of landslides: from creeping behaviour to catastrophic failure. Géotechnique 66, 202–219 (2016).

43. Handwerger, A. L., Rempel, A. W., Skarbek, R. M., Roering, J. J. & Hilley, G. E. Rate-weakening friction characterizes both slow sliding and catastrophic failure of landslides. Proc. Natl. Acad. Sci. 113, 10281–10286 (2016).

44. Prevost, J. H. A simple plasticity theory for frictional cohesionless soils. Int. J. Soil. Dyn. Earthq. Eng. 4, 9–17 (1985).

45. Comegna, L., Picarelli, L. & Urciuoli, G. The mechanics of mudslides as a cyclic undrained-drained process. Landslides 4, 217–232 (2007).

46. Di Maio, C., De Rosa, J., Vassallo, R., Coviello, R., & Macchia, G. Hydraulic conductivity and pore water pressures in a clayey landslide: Experimental data. Geoscience 10, 102 https://doi.org/10.3390/geosciences10030102 (2020).

47. Miao, H. & Wang, G. Shear rate effect on the residual strength of saturated clayey and granular soils under low- to high-rate continuous shearing. Eng. Geol. 308, 106821 (2022).

48. Corominas, J., Moya, J., Ledesma, A., Lloret, A. & Gili, J. A. Prediction of ground displacements and velocities from groundwater level changes at the Vallcebre landslide (Eastern Pyrenees, Spain). Landslides 2, 83–96 (2005).

49. Oberender, P. W. & Puzrin, A. M. Observation-guided constitutive modelling for creeping landslides. Géotechnique 66, 232–247 (2016).

50. van Asch, T. W. J., Van Beek, L. P. H. & Bogaard, T. A. Problems in predicting the mobility of slow-moving landslides. Eng. Geol. 91, 46–55 (2007).

51. Hungr, O., Leroueil, S. & Picarelli, L. The Varnes classification of landslide types, an update. Landslides 11, 167–194 (2014). Nov.

52. von Terzaghi, K. Erdbaumechanik auf bodenphysikalischer Grundlage. Leipzig-Wien: Franz Deuticke, (1925).

53. Picarelli, L., Olivares, L., Comegna, L. & Damiano, E. Mechanical aspects of flow-like movements in granular and fine grained soils. Rock. Mech. Rock Eng. 41, 179–197 (2008).

54. Rosone, M., Ziccarelli, M., Ferrari, A. & Farulla, C. A. On the reactivation of a large landslide induced by rainfall in highly fissured clays. Eng. Geol. 235, 20–38 (2018).

55. Wang, G. & Sassa, K. Post-failure mobility of saturated sands in undrained load-controlled ring shear tests. Can. Geotech. J. 39, 821–837 (2002).

56. L. Luzi et al. "Engineering Strong Motion database (ESM) (Version 2.0)", Istituto Nazionale di Geofisica e Vulcanologia. 2020. [Online]. Available: https://doi.org/10.13127/ESM.2.

57. Wang, C. Y. & Chia, Y. Mechanism of water level changes during earthquakes: Near field versus intermediate field. Geophys. Res. Lett. 35, 12402 (2008).

58. Legros, F. The mobility of long-runout landslides. Eng. Geol. 63, 301–331 (2002).

59. Handwerger, A. L. et al. Widespread Initiation, Reactivation, and Acceleration of Landslides in the Northern California Coast Ranges due to Extreme Rainfall. J. Geophys. Res. Earth Surf. 124, 1782–1797 (2019).

60. Alvarado, M., Pinyol, N. M. & Alonso, E. E. Landslide motion assessment including rate effects and thermal interactions: Revisiting the canelles landslide. Can. Geotech. J. 56, 1338–1350 (2019).

61. Zhang, S. & Zhang, L. M. Impact of the 2008 Wenchuan earthquake in China on subsequent long-term debris flow activities in the epicentral area. Geomorphology 276, 86–103 (2017).

62. Iverson, R. M. Regulation of landslide motion by dilatancy and pore pressure feedback. J. Geophys. Res. Earth Surf. 110, 2015 (2005).

63. Iverson, R. M. et al. Acute sensitivity of landslide rates to initial soil porosity. Sci. 290, 513–516 (2000).

64. Lemos, L. J. & Vaughan, P. R. Clay - interface shear resistance. Géotechnique 50, 55–64 (2000).

65. Zienkiewicz, O.C. Dynamic behaviour of saturated porous media; The generalized Biot formulation and its numerical solution.pdf. Int. J. Numer. Anal. Methods Geomech. 8, 71–96 https://doi.org/10.1002/nag.1610080106 (1984).

66. Zienkiewicz, O. C., Chang, C. T. & Bettess, P. Drained, undrained, consolidating and dynamic behaviour assumptions in soils. Geotechnique 30, 385–395 (1980).

67. Sandhu, R. S., Liu, H. & Singh, K. J. Numerical performance of some finite element schemes for analysis of seepage in porous elastic media. Int. J. Numer. Anal. Methods Geomech. 1, 177–194 (1977).

68. Reed, M. B. An investigation of numerical errors in the analysis of consolidation by finite elements. Int. J. Numer. Anal. Methods Geomech. 8, 243–257 (1984).

69. Zienkiewicz, O.C., Bicanic, N., & Shen, F.Q. Earthquake Input Definition and the Trasmitting Boundary Conditions, in Advances in Computational Nonlinear Mechanics, Vienna: Springer Vienna, 1989, 109–138.

70. Lysmer, J. & Kuhlemeyer, R. L. Finite Difference Model for Infinite Media. J. Eng. Mech. 95, 859–877 (1969).

71. Mejia, L. H., & Dawson, E. M. Earthquake deconvolution for FLAC. Proceedings of the 4th International FLAC symposium on numerical modeling in geomechanics. 4–10 (2006).

72. Duong, N. T., Suzuki, M. & Van Hai, N. Rate and acceleration effects on residual strength of kaolin and kaolin–bentonite mixtures in ring shearing. Soils Found. 58, 1153–1172 (2018).

73. Puzrin, A. M. & Schmid, A. Progressive failure of a constrained creeping landslide. Proc. R. Soc. A Math. Phys. Eng. Sci. 467, 2444–2461 (2011).

74. Stoecklin, A., Friedli, B., & Puzrin, A.M. A multisurface kinematic hardening model for the behavior of clays under combined static and undrained cyclic loading. *Int. J. Numer. Anal. Methods Geomech*. **44**, 2358–2387 https://doi.org/10.1002/nag.3149 (2020).

75. Elgamal, A., Yang, Z., Parra, E. & Ragheb, A. Modeling of cyclic mobility in saturated cohesionless soils. *Int. J. Plast.* **19**, 883–905 (2003).

76. Bekaert, D. P. S., Handwerger, A. L., Agram & Kirschbaum, D. B. InSAR-based detection method for mapping and monitoring slow-moving landslides in remote regions with steep and mountainous terrain: An application to Nepal. *Remote. Sens. Environ.* **249**, 111983 (2020).

77. Hardin, B. O. & Richart, F. E. Jr. Elastic Wave Velocities in Granular Soils. *J. Soil. Mech. Found. Div.* **89**, 33–65 (1963).

Acknowledgements

Author contributions

M.K. developed the coupled FE code, implemented the constitutive models, ran all the simulations and prepared the figures and the manuscript. A.M.P. as the project leader contributed conceptually and to writing the manuscript.

Competing interests

The authors declare no competing interests.

Additional information

Supplementary information The online version contains supplementary material available at https://doi.org/10.1038/s43247-023-00797-3.

Correspondence and requests for materials should be addressed to Marc Kohler.

Peer review information *Communications Earth & Environment* thanks Roland Burgmann and the other, anonymous, reviewer(s) for their contribution to the peer review of this work. Primary Handling Editors: Sylvain Barbot and Joe Aslin.

Reprints and permission information is available at http://www.nature.com/reprints

Publisher's note Springer Nature remains neutral with regard to jurisdictional claims in published maps and institutional affiliations.